

# Solving Quadratic Programs via Deep Unrolled Douglas-Rachford Splitting

Anonymous authors

Paper under double-blind review

## Abstract

Convex quadratic programs (QPs) are fundamental to numerous applications, including finance, engineering, and energy systems. Among the various methods for solving them, the Douglas-Rachford (DR) splitting algorithm is notable for its robust convergence properties. Concurrently, the emerging field of Learning-to-Optimize offers promising avenues for enhancing algorithmic performance, with algorithm unrolling receiving considerable attention due to its computational efficiency and interpretability. In this work, we propose an approach that unrolls a modified DR splitting algorithm to efficiently learn solutions for convex QPs. Specifically, we introduce a tailored DR splitting algorithm that replaces the computationally expensive linear system-solving step with a simplified gradient-based update, while retaining convergence guarantees. Consequently, we unroll the resulting DR splitting method and present a well-crafted neural network architecture to predict QP solutions. Our method achieves up to 50% reductions in iteration counts and 40% in solve time across benchmarks on both synthetic and real-world QP datasets, demonstrating its scalability and superior performance in enhancing computational efficiency across varying sizes.

## 1 Introduction

Convex Quadratic Programs (QPs) are optimization problems characterized by a convex quadratic objective function and linear constraints. These problems form a fundamental class of optimization tasks with applications spanning finance (Markowitz, 1952; Boyd et al., 2017), engineering (Garcia et al., 1989), energy systems (Frank & Rebennack, 2016), and machine learning (Cortes, 1995; Tibshirani, 1996). Additionally, convex QPs serve as the basis for constructing sequential convex approximations or relaxations of nonconvex problems, ensuring tractable subproblems while progressively approaching high-quality solutions (Boyd & Vandenberghe, 2004).

In recent years, there has been increasing interest in the development of *first-order methods* for convex QPs, with OSQP (Stellato et al., 2020) and Splitting Conic Solver (SCS) (O’Donoghue, 2021) standing out as state-of-the-art solvers. These methods are closely related to the classical Douglas-Rachford (DR) splitting algorithm (Douglas & Rachford, 1956). Notably, they require only a few matrix factorizations, which can be reused across iterations. More recently, Lu & Yang (2023) extended the Primal-Dual Hybrid Gradient (PDHG) algorithm to effectively solve convex QPs without requiring any matrix factorization. These first-order methods have demonstrated superior efficiency compared to traditional approaches like Active-Set methods (Wolfe, 1959) and Interior Point Methods (IPMs) (Nesterov & Nemirovskii, 1994), especially for large-scale problems.

With the emergence of *Learn-to-Optimize* (L2O) methods, innovative strategies have been proposed to accelerate the solving of optimization problems (Chen et al., 2022; Gasse et al., 2022). By training models on diverse problem instances, L2O aims to learn problem-specific optimization strategies that surpass traditional methods in terms of efficiency and performance. In particular, the recent work of Yang et al. (2024) proposed to unroll the matrix-free PDHG algorithm in Lu & Yang (2023). This approach enables a relatively shallow network to efficiently learn the optimal QP solutions that would otherwise require thousands of PDHG iter-

ations. However, directly unrolling DR splitting-based algorithms to efficiently learn QP solutions presents challenges, primarily due to the need to solve a linear system at each iteration. This raises the following question:

*How to unroll DR splitting-based algorithms for solving convex QPs?*

In this work, we propose unrolling a modified DR splitting algorithm in which the linear system-solving step is replaced by an equivalent least-squares problem, eliminating the need for matrix factorization. Rather than solving the least-squares problem exactly, we apply a single-step gradient descent update. Consequently, the tailored DR splitting algorithm can be seamlessly unrolled into a learnable network, delivering high-quality solutions for convex QPs. The distinct contributions of this work are as follows:

- **Unrolled DR Splitting:** We present a well-crafted neural network framework that leverages the unrolling of a modified DR splitting algorithm to efficiently solve convex QPs.
- **Convergence Guarantee:** We present the convergence properties of the modified DR splitting algorithm and demonstrate that the unrolled network can recover the optimal QP solutions.
- **Empirical Evaluation:** We validate the proposed framework through extensive experiments. The resulting solutions are employed to warm-start the QP solver SCS. The results indicate that our method significantly enhances the efficiency of solving convex QPs. In particular, our approach reduces the number of iterations by up to 50% and the solve time by up to 40%, demonstrating its effectiveness across diverse benchmarks.

## 2 Related Works

**Learning-Accelerated QP Algorithms.** Recently, machine learning techniques have been applied to develop more effective policies within algorithms, surpassing the performance of traditional hand-crafted heuristic methods. For example, Ichnowski et al. (2021); Jung et al. (2022) employed reinforcement learning to choose hyperparameters in the OSQP solver, leading to faster convergence compared to the original update rules. Venkataraman & Amos used neural networks to learn acceleration methods in fixed-point algorithms. While both approaches demonstrated improved convergence rates empirically, the convergence can not be theoretically ensured.

**Algorithm Unrolling.** Algorithm unrolling is a technique that bridges classical iterative optimization methods and deep learning by transforming the iterative steps of an optimization algorithm into the layers of a neural network. This approach enables end-to-end training, combining the strengths of both paradigms. Unrolled networks are not only interpretable, but they also tend to require fewer parameters and less training data compared to traditional deep learning models (Monga et al., 2021). By leveraging a few layers of unrolled networks, these methods can often learn solutions that would otherwise require thousands of iterations in classical algorithms. Significant success has been achieved in applications such as sparse coding (Gregor & LeCun, 2010), compressive sensing (Xie et al., 2019) and communication systems (Sun et al., 2023). However, these methods are not applicable to general optimization algorithms. Recently, Li et al. (2024); Yang et al. (2024) proposed unrolling the PDHG algorithm into neural networks to address general linear programs and QPs, establishing theoretical results in this context. To the best of our knowledge, such theoretical advancements have not been extended to other efficient first-order methods, such as DR splitting-based algorithms.

**Learning Warm-Starts.** An effective strategy to accelerate solution processes is to provide high-quality initializations. For example, Baker (2019); Diehl (2019); Zhang & Zhang (2022) proposed predicting initial points to warm-start the solution process for power system applications. However, these methods mainly focus on solution mappings and do not address the specific needs of warm-starting nonlinear programming algorithms. Highly related works of Sambharya et al. (2023; 2024) train fully-connected neural networks by minimizing loss after taking several steps of the fixed-point algorithms. By incorporating additional algorithmic steps following the warm-start, the predictions are refined for downstream processes. However,

due to the need for vectorizing problem parameters and solving linear systems during training, this method would struggle when addressing large-scale problems. In contrast to fixed-point algorithms, Gao et al. (2024) introduced IPM-LSTM, which replaces the time-consuming process of solving linear systems in IPMs with Long Short-Term Memory (LSTM) neural networks. While this approach shows promise in providing well-centered primal-dual solution pairs for warm-starting IPM solvers, the overhead of LSTM inference limits its scalability to larger instances.

### 3 Preliminaries

#### 3.1 Quadratic Programs

In this work, we consider convex QPs of the following form:

$$\begin{aligned} \min_{x \in \mathbb{R}^n, s \in \mathcal{K}} \quad & \frac{1}{2}x^\top Px + c^\top x \\ \text{s.t.} \quad & Ax + s = b, \\ & s \in \mathcal{K}, \end{aligned} \tag{1}$$

where  $P \in \mathbb{R}^{n \times n}$ ,  $P = P^\top \succeq 0$ ,  $A \in \mathbb{R}^{m \times n}$ ,  $c \in \mathbb{R}^n$ , and  $b \in \mathbb{R}^m$  are the problem parameters, with  $x \in \mathbb{R}^n$  and  $s \in \mathcal{K} := \mathbb{R}_+^m$  denoting decision variables.

#### 3.2 Douglas-Rachford Splitting

For convex QPs, the following Karush-Kuhn-Tucker (KKT) conditions are necessary and sufficient for optimality:

$$\begin{aligned} Ax + s &= b, & Px + A^\top y + c &= 0, \\ s &\in \mathcal{K}, y &\in \mathcal{K}^*, & s \perp y, \end{aligned}$$

where  $y$  is the dual variable and  $\mathcal{K}^*$  is the dual cone to  $\mathcal{K}$ , defined as  $\mathcal{K}^* = \{v \mid v^\top z \geq 0, \forall z \in \mathcal{K}\}$ . Let

$$\begin{aligned} u &:= \begin{bmatrix} x \\ y \end{bmatrix}, & M &:= \begin{bmatrix} P & A^\top \\ -A & 0 \end{bmatrix}, \\ q &:= \begin{bmatrix} c \\ b \end{bmatrix}, & \mathcal{C} &:= \mathbb{R}^n \times \mathcal{K}^*. \end{aligned}$$

Since  $P \succeq 0$ ,  $M + M^\top \succeq 0$ , i.e.,  $M$  is monotone. Consequently, the KKT conditions can be expressed as the following monotone inclusion problem:

$$0 \in Mu + q + N_{\mathcal{C}}(u), \tag{2}$$

where  $N_{\mathcal{C}}(u)$  represents the normal cone of  $\mathcal{C}$ , and is defined by

$$N_{\mathcal{C}}(u) := \begin{cases} \{v \mid (z - u)^\top v \leq 0, \quad \forall z \in \mathcal{C}\}, & u \in \mathcal{C}, \\ \emptyset, & u \notin \mathcal{C}. \end{cases}$$

The optimal solutions for problem (1) can thus be obtained by solving the monotone inclusion problem (2).

To address problem (2), the well-known DR splitting algorithm (Douglas & Rachford, 1956), as outlined in Algorithm 1, can be applied. In each iteration, an intermediate point  $\tilde{u}^{k+1}$  is computed by solving a linear system, which is always solvable due to the full rank of  $I + M$ . The updated point  $u^{k+1}$  is then obtained by reflecting  $\tilde{u}^{k+1}$  around  $w^k$  and projecting it onto the conic set  $\mathcal{C}$  using  $\Pi_{\mathcal{C}}$ . Finally, the iterate  $w^{k+1}$  is updated by combining  $w^k$ ,  $u^{k+1}$ , and  $\tilde{u}^{k+1}$ , balancing objective minimization with constraint satisfaction. Let  $u^*$  be the optimal solution to problem (2), if it exists. Then  $u^k \rightarrow u^*$  as  $k \rightarrow \infty$ . Additionally, the residual  $\|w^{k+1} - w^k\|^2 \rightarrow 0$  at a rate of  $\mathcal{O}(1/k)$  (He & Yuan, 2015; Davis & Yin, 2016).

**Algorithm 1** Douglas-Rachford Splitting

---

```

1: Input:  $M, q, \mathcal{C}$ 
2: Initialize:  $w^0 \leftarrow \mathbf{0}$ 
3: for  $k = 0, 1, \dots$  do
4:    $\tilde{u}^{k+1} \leftarrow (I + M)^{-1}(w^k - q)$ 
5:    $u^{k+1} \leftarrow \Pi_{\mathcal{C}}(2\tilde{u}^{k+1} - w^k)$ 
6:    $w^{k+1} \leftarrow w^k + (u^{k+1} - \tilde{u}^{k+1})$ 
7: end for
8: Return:  $u^k := (x^k, y^k)$ 

```

---

**4 Deep Unrolled DR Splitting**

In this work, we aim to design a neural network architecture that efficiently learns high-quality solutions for convex QPs. However, directly unrolling Algorithm 1 presents challenges due to the need to solve linear systems in Step 4. To address this, we first introduce the DR-GD algorithm. Building on this foundation, we then present the unrolled neural network framework.

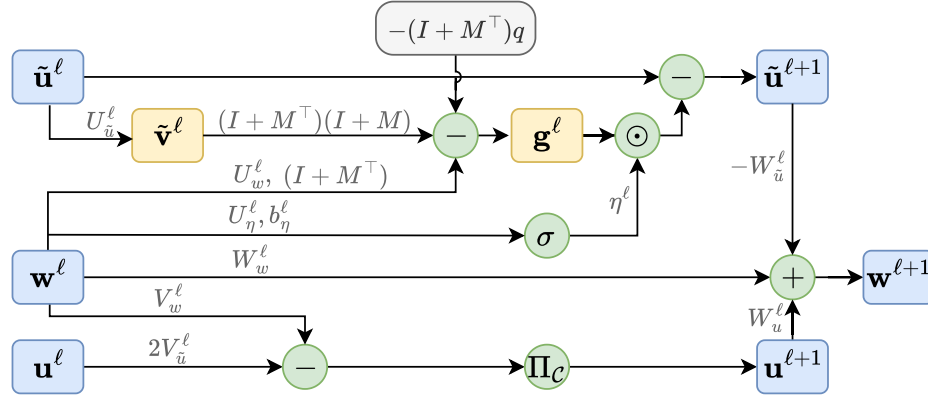


Figure 1: One layer of the proposed DR-GD Net.

**4.1 DR-GD Algorithm****Algorithm 2** DR-GD Algorithm

---

```

1: Input:  $M, q, \mathcal{C}$ 
2: Initialize:  $w^0 \leftarrow \mathbf{0}, \tilde{u}^0 \leftarrow \mathbf{0}$ 
3: for  $k = 0, 1, \dots$  do
4:    $t^k \leftarrow (I + M)^\top((I + M)\tilde{u}^k - (w^k - q))$ 
5:   Compute  $\eta^k$  by line search
6:    $\tilde{u}^{k+1} \leftarrow \tilde{u}^k - \eta^k t^k$ 
7:    $u^{k+1} \leftarrow \Pi_{\mathcal{C}}(2\tilde{u}^{k+1} - w^k)$ 
8:    $w^{k+1} \leftarrow w^k + (u^{k+1} - \tilde{u}^{k+1})$ 
9: end for
10: Return  $u^k := (x^k, y^k)$ 

```

---

Solving linear systems is often achieved via *direct methods* or *indirect methods* (Stellato et al., 2020; O’Donoghue, 2021). However, significant challenges arise when unrolling Algorithm 1 with linear systems being solved by either method.

- *Direct method*: The direct method involves matrix factorization, where dynamic pivoting is used, making the sequence of operations data-dependent and, therefore, not known in advance. This adaptive nature complicates the task of breaking the algorithm into a fixed, unrolled architecture.
- *Indirect method*: The indirect method, in contrast, employs iterative algorithms, such as the conjugate gradient descent method, to solve the linear systems. While this approach circumvents the need for matrix factorization, it introduces the complexity of inner-outer iterations, complicating the unrolling process.

Since  $I + M$  is invertible, solving the linear system in Step 4 of Algorithm 1 is equivalent to addressing the following unconstrained *least-squares problem*:

$$\min_{\tilde{u}} f(\tilde{u}) := \frac{1}{2} \|(I + M)\tilde{u} - (w^k - q)\|^2. \quad (3)$$

Moreover, provided that the  $\ell^2$ -norm of the error in solving the linear systems in Step 4 is finitely summable, Algorithm 1 guarantees convergence to optimal solutions (Eckstein & Bertsekas, 1992; Combettes, 2004). If problem (3) is solved to a pre-specified accuracy using iterative methods, unrolling Algorithm 1 results in a nested architecture due to the inner-outer iterations. The need to replicate the iterative process increases complexity and reduces efficiency, making the unrolled network more difficult to scale. In this work, we streamline the process by employing a single gradient step,  $\tilde{u}^{k+1} \leftarrow \tilde{u}^k - \eta^k \nabla f(\tilde{u}^k)$ , at each iteration, where  $\tilde{u}^k$  denotes the previous iterate and  $\eta^k$  is the step size. This gradient-based update enhances both efficiency and scalability when unrolled. The resulting algorithm is outlined in Algorithm 2.

**Proposition 1.** *The sequence  $\{u^k\}$  generated by Algorithm 2 converges to the solution of problem (2). Furthermore, the sequences  $\{x^k\}$  and  $\{y^k\}$  also converge to the solution of problem (1).*

In Proposition 1, we demonstrate that Algorithm 2 converges to the optimal solution of problem (1), with the proof provided in Appendix A. While Algorithm 2 is expected to converge at a slower rate than Algorithm 1 due to the inexact evaluation involved in solving linear systems, it offers significant advantages in terms of unrolling and parameterization by eliminating the need for matrix factorizations or innerouter iterations.

## 4.2 Algorithm Unrolling

---

### Algorithm 3 DR-GD Net

---

```

1: Input:  $M, q, \mathcal{C}$ , number of layers  $L$  and embedding size  $d^\ell$ .
2: Initialize:  $\tilde{\mathbf{u}}^0 \leftarrow \mathbf{0}, \mathbf{u}^0 \leftarrow \Pi_{\mathcal{C}}(-\mathbf{q}), \mathbf{w}^0 \leftarrow q \cdot \mathbf{1}^{d^0} + \mathbf{u}^0$ ;
3: for  $\ell = 1, \dots, L$  do
4:   Update  $\tilde{u}$ :  $\tilde{\mathbf{v}}^\ell \leftarrow \tilde{\mathbf{u}}^{\ell-1} U_{\tilde{u}}^\ell$ ;
5:    $\mathbf{g}^\ell \leftarrow (I + M)^\top \left( (I + M)\tilde{\mathbf{v}}^\ell - \left( \mathbf{w}^{\ell-1} U_w^\ell - q \cdot \mathbf{1}^{d^\ell} \right) \right)$ ;
6:    $\tilde{\mathbf{u}}^\ell \leftarrow \tilde{\mathbf{v}}^\ell - \eta^\ell \sigma \left( \mathbf{w}^{\ell-1} U_\eta^\ell + b_\eta^\ell \right) \odot \mathbf{g}^\ell$ ;
7:   Update  $u$ :  $\mathbf{u}^\ell \leftarrow \Pi_{\mathcal{C}} \left( 2\tilde{\mathbf{u}}^\ell V_{\tilde{u}}^\ell - \mathbf{w}^{\ell-1} V_w^\ell \right)$ ;
8:   Update  $w$ :  $\mathbf{w}^\ell \leftarrow \mathbf{w}^{\ell-1} W_w^\ell + \left( \mathbf{u}^\ell W_u^\ell - \tilde{\mathbf{u}}^\ell W_{\tilde{u}}^\ell \right)$ 
9: end for
10: Return  $u := \mathbf{u}^L P_u^{L+1}$ 

```

---

In this section, we propose DR-GD Net which is designed by unrolling Algorithm 2. The structure of the model is detailed in Algorithm 3, where parameters for channel expansion are introduced to enhance the model’s flexibility and learning capacity.  $\mathbf{1}^d$  is a row vector with all ones in dimension  $d$ ,  $\tilde{\mathbf{u}}^0, \mathbf{u}^0$  and  $\mathbf{w}^0 \in \mathbb{R}^{(n+m) \times d^0}$ . Let  $\Theta := \left\{ \{\theta_{\tilde{u}}^\ell, \theta_u^\ell, \theta_w^\ell\}_{\ell=1}^L, P_u^{L+1} \right\}$  be the parameters of the network, where  $\theta_{\tilde{u}}^\ell := (U_{\tilde{u}}^\ell, U_w^\ell, U_\eta^\ell, b_\eta^\ell)$ ,  $\theta_u^\ell := (V_{\tilde{u}}^\ell, V_w^\ell)$  and  $\theta_w^\ell := (W_w^\ell, W_u^\ell, W_{\tilde{u}}^\ell)$ .  $\eta^\ell \in \mathbb{R}$  is the prior knowledge about the step-size of the  $\ell$ -th layer.  $P_u^{L+1}$  is the final linear mapping for the outputs.  $\sigma(\cdot)$  is the sigmoid activation function. The projection operator  $\Pi_{\mathcal{C}}$  can be implemented by using the ReLU activation function. One layer of DR-GD Net is depicted in Figure 1.

Specifically, the unrolled DR-GD Net can emulate Algorithm 2 by applying specific instantiation of  $\Theta$ . Consequently, Algorithm 3 is capable of recovering the optimal solutions to problem (1) when an adequate number of layers are employed. However, by introducing learnable parameters, our goal is to allow the network to adapt to different problem instances, thereby enabling it to achieve approximate solutions with much fewer layers.

### 4.3 Training

In this work, the neural network is trained in a supervised manner, with the loss function defined as the  $\ell^2$  distance between the predicted primal-dual solutions  $(x, y)$  and the optimal solutions  $(x^*, y^*)$ , obtained by solving QPs using the SCS solver.

For a dataset of QPs,  $\mathcal{M}$ , we train the proposed network by finding the optimal  $\Theta$  by minimizing the following loss function:

$$\min_{\Theta} \frac{1}{2|\mathcal{M}|} \sum_{i=1}^{|\mathcal{M}|} (\|x_i - x_i^*\|^2 + \|y_i - y_i^*\|^2),$$

where the subscript  $i$  indicates the  $i^{th}$  sample in  $\mathcal{M}$ .

In the recent works of Sambharya et al. (2023; 2024), an unsupervised loss function based on the fixed-point residual was proposed, which eliminates the need for labeled data. However, as noted in Sambharya et al. (2024), this approach tends to focus localized optimization metrics within the iterative process rather than the overall objective, potentially limiting its effectiveness; that is, the loss values may appear sufficiently low even when the solutions produced are far from optimal. By leveraging supervised learning with a regression loss, the DR-GD Net can learn an effective warm-start point, enhancing the performance of downstream DR splitting-based algorithms. This approach not only aligns the network architecture with the underlying algorithm but also incorporates the global insights provided by the ground truth optimal solutions.

## 5 Computational Studies

To evaluate the proposed framework, we first analyze the convergence behavior of Algorithm 2 on synthetic instances of varying sizes. Next, we compare its performance against state-of-the-art solvers and learning-based baselines on both synthetic and real-world datasets. Finally, we provide a detailed discussion of the results. The code is publicly available at <https://anonymous.4open.science/r/DR-GD-722B/>.

**Baseline Algorithms.** In our experiments, we denote our algorithm as DR-GD-NN and compare it against state-of-the-art solvers and L2O algorithms.

The solvers considered are:

- (i) **SCS** (O’Donoghue, 2021): A first-order solver for quadratic cone programming based on the DR splitting algorithm with homogeneous self-dual embedding.
- (ii) **OSQP** (Stellato et al., 2020): A first-order convex QP solver based on the alternating direction method of multipliers, which is equivalent to DR splitting under appropriate variable transformations.

For **SCS**, the default linear solver is used with an absolute feasibility tolerance of  $10^{-4}$ , relative feasibility tolerance of  $10^{-4}$ , and infeasibility tolerance of  $10^{-7}$ . **SCS** also employs techniques such as adaptive step sizing, over-relaxation, and data normalization to enhance performance. Further details can be found in O’Donoghue (2021).

Unlike **SCS**, **OSQP** enforces only primal and dual feasibility without explicitly verifying the termination criteria based on the primal-dual gap. To ensure a fair comparison, we follow the approach in Lu & Yang (2023); O’Donoghue (2021) to obtain **OSQP** solutions within the desired gap tolerance. Specifically, we initialize absolute and relative feasibility tolerances at  $10^{-4}$  (as in **SCS**) and iteratively halve them if the gap tolerance

is not met. Additionally, the convergence-checking interval is set to be 1 for both SCS and OSQP in all experiments.

The learning-based baseline algorithms include:

- (i) **L2WS(Fp)** (Sambharya et al., 2024): A feedforward neural network that takes vectorized instance parameters as input to generate warm starts, followed by 60 fixed algorithmic iterations, as suggested in Sambharya et al. (2024). The network is trained with the fixed-point residual as the unsupervised loss function.
- (ii) **L2WS(Reg)** (Sambharya et al., 2024): A method that shares the same architecture and number of iterations as L2WS(Fp) but employs a regression loss function instead.
- (iii) **GNN** (Chen et al., 2024): A graph neural network trained using a regression loss on graphs representing the QP instances.

**Datasets.** The datasets used in this work include synthetic benchmarks and perturbed real-world instances. Specifically, the datasets are:

- (i) **QP (RHS)** (Donti et al., 2021): Convex QPs parameterized only by the right-hand side of equality constraints, generated as in Donti et al. (2021), with  $n = 200, 500, 1000$  in the experiments.
- (ii) **QP** (Gao et al., 2024): The dataset generated as in Gao et al. (2024), where all the parameters are perturbed by a random factor sampled from  $U[0.9, 1.1]$ .
- (iii) **QPLIB** (Furini et al., 2019): Selected instances from Furini et al. (2019) with all parameters perturbed by a random factor sampled from  $U[0.9, 1.1]$ .
- (iv) **Portfolio** (Stellato et al., 2020): Consider the portfolio optimization problem, as introduced in Stellato et al. (2020), which is formulated as follows:

$$\begin{aligned}
 \min_{x \in \mathbb{R}^n, y \in \mathbb{R}^k} \quad & x^\top D x + y^\top y - \frac{1}{\gamma} \mu^\top x \\
 \text{s.t.} \quad & y = F^\top x \\
 & \mathbf{1}^\top x = 1 \\
 & x \geq 0
 \end{aligned}$$

where the variable  $x \in \mathbb{R}^n$  represents the portfolio,  $y \in \mathbb{R}^k$  is the axillary variable. The problem is parameterized by  $\mu \in \mathbb{R}^n$  the vector of expected returns,  $\gamma > 0$  the risk aversion parameter,  $F \in \mathbb{R}^{n \times k}$  the factor loading matrix and  $D \in \mathbb{R}^{n \times n}$  a diagonal matrix describing the asset-specific risk. The problems with  $k = 100, 200, 300, 400$  factors and  $n = 10k$  assets are considered in the experiments. The instances are generated by sampling  $F_{ij} \sim N(0, 1)$  with 50% nonzero elements,  $D_{ii} \sim U[0, \sqrt{k}]$ ,  $\mu_i \sim N(0, 1)$  and  $\gamma = 1$ .

All instances considered in this work are formulated as in (4).

$$\begin{aligned}
 \min_{x \in \mathbb{R}^n} \quad & \frac{1}{2} x^\top P x + c^\top x \\
 \text{s.t.} \quad & A x = b \\
 & G x \leq h \\
 & l \leq x \leq u
 \end{aligned} \tag{4}$$

where  $P = P^\top \succeq 0, c \in \mathbb{R}^n, A \in \mathbb{R}^{m_1 \times n}, b \in \mathbb{R}^{m_1}, G \in \mathbb{R}^{m'_2 \times n}, h \in \mathbb{R}^{m'_2}$  are the model parameters. The bounds on the variables are given by  $l, u \in \mathbb{R}^n$ . The formulation in problem (4) can be transformed into problem (1) by integrating the bound constraints into inequality constraints and merging the equality and inequality constraints. The size of each dataset is listed in Table 1.

For each dataset, 400 samples are generated for training, 40 for validation, and 100 for testing. All reported results are based on the test set.

Table 1: Problem sizes

Instance		$n$	$m_1$	$m_2$
<b>QP (RHS)</b>	$N$	$N$	$N/2$	$N/2$
<b>QP</b>	$N$	$N$	$N/2$	$N/2$
<b>QPLIB</b>	3913	300	61	600
	8845	1,546	490	1,848
	4270	1,600	401	3,202
	3547	1,998	89	2,959
<b>Portfolio</b>	$k$	$11k$	$k + 1$	$20k$

**Evaluation Configurations.** All experiments were conducted on an NVIDIA GeForce RTX 3090 GPU and a 12th Gen Intel(R) Core(TM) i9-12900K CPU, using Python 3.9.17, PyTorch 2.0.1, SCS 3.2.6 (O’Donoghue, 2021) and OSQP 0.6.7 (Stellato et al., 2020). To demonstrate the warm-start effect across various solver configurations and ensure experimental consistency with baseline methods, we explored different parameter settings for SCS on each dataset, as detailed in Appendix B.

In all experiments, DR-GD Nets with 4 layers and embedding sizes of 128 are trained with a batch size of 2, a learning rate of  $10^{-5}$ , and the Adam optimizer (Kingma, 2014). The parameters  $\eta^l$  are set to 0.05 for QPLIB datasets and 0.1 for the other datasets. Early stopping is employed to terminate training if the validation loss shows no improvement for 10 consecutive epochs. The model achieving the best validation performance is saved for testing.

### 5.1 Convergence of DR-GD

This section analyzes the convergence behavior of Algorithm 2, the foundation of our proposed DR-GD Net. The convergence of Algorithm 2 is expected to be slower than Algorithm 1, due to the inexact evaluation at each iteration. In Table 2, we compare the performance of Algorithm 1 and Algorithm 2 on the dataset **QP** with different sizes, with a stopping criterion of  $1 \times 10^{-6}$  for the fixed-point error  $\|w^{k+1} - w^k\|_2$ . The columns “Obj.”, “Max Eq.”, “Max Ineq.”, and “Iter.” report the objective value, maximum equality constraint violation, maximum inequality constraint violation, and number of iterations upon termination, respectively. The “Ratio” column shows the ratio of the number of iterations required by Algorithm 2 to those required by Algorithm 1.

The results indicate that, Algorithm 2 could produce solutions with the desired feasibility and optimality, though it generally requires more iterations than the original DR splitting algorithm. The computational overhead remains manageable with a maximum factor of 1.50 and decreases as the problem size increases. Despite its slower convergence, Algorithm 2 avoids exact computation of linear systems, making it well-suited for the development of an unrolled neural network based on this approach.

Table 2: Convergence comparison between Algorithm 1 and Algorithm 2

Instance	Algorithm 1				Algorithm 2				Ratio	
	Obj.	Max Eq.	Max Ineq.	Iter.	Obj.	Max Eq.	Max Ineq.	Iter.		
QP	200	−37.126	$4.0 \times 10^{-10}$	$4.6 \times 10^{-10}$	5,049	−37.126	$2.4 \times 10^{-6}$	$1.4 \times 10^{-6}$	7,555	1.50
	500	−90.878	$1.2 \times 10^{-10}$	$8.7 \times 10^{-11}$	13,653	−90.878	$2.0 \times 10^{-6}$	$1.6 \times 10^{-6}$	16,523	1.21
	1000	−160.185	$3.8 \times 10^{-11}$	$3.2 \times 10^{-11}$	30,844	−160.185	$2.6 \times 10^{-7}$	$2.0 \times 10^{-6}$	36,280	1.18

### 5.2 Computational Results on DR-GD Net

**QP (RHS).** We compare the warm-start performance of L2WS(FP), L2WS(Reg), GNN, and DR-GD-NN on the **QP (RHS)** test set across various problem sizes. The instances are parameterized by the right-hand sides of



the equality constraints, encapsulated in a single vector that serves as the input to the neural network in the L2WS models. The results are summarized in Table 3. The column labeled “Cold Start” shows the number of iterations and the solve time required by the SCS solver without warm starts. The “Iters.”/ “Time (s)” and “Ratio” columns present the iterations/total time (including model inference and solve time in seconds) and the average reduction ratio achieved by each method across all test problems. To align the experiment settings of baseline methods, solver settings were configured with advanced techniques disabled, as shown in Table 6. The best results in each category are highlighted in bold.

Overall, L2WS(Reg) and DR-GD-NN demonstrate comparable performance. Specifically, L2WS(Reg) achieves the best results on instances with 200 variables, where the simple right-hand-side perturbation facilitates learning the mapping from parameters to warm-start points. However, as the problem scale increases, DR-GD-NN surpasses L2WS(Reg), achieving a 45.4% and 53.6% reduction in iterations for datasets with 500 and 1000 variables, respectively. This highlights the efficiency of DR-GD-NN in handling larger instances, where the increased input size adds complexity to the solution mapping for L2WS. The L2WS(FP) variant is generally outperformed by L2WS(Reg), except in the smallest case with 100 variables. This result demonstrates the superiority of using a regression loss over the unsupervised fixed-point residual loss, which primarily focuses on intermediate metrics within the iterative process. This could potentially lead L2WS(FP) to converge to suboptimal regions, particularly in larger and more complex problems. In contrast, the regression loss leverages global information from ground-truth solutions, enabling better performance across a broader range of problem sizes and complexities. Additionally, while GNN performs competitively on instances with 200 variables, it falls short on larger datasets compared to DR-GD-NN.

In terms of solution time, the proposed method consistently outperforms the baseline approaches, achieving reductions of up to 53.5%. Notably, even under some rare cases where the reduction in iterations is not the largest, DR-GD-NN still demonstrates superior efficiency. This advantage is attributed to the fast inference time of the proposed framework, which eliminates the need for the additional iterative steps required by the L2WS methods. For smaller instances, the reduction in the solving time is less pronounced compared to larger problems, probably because the shorter solving time for small instances leaves less room for improvement.

Table 3: Comparison of results on **QP (RHS)** dataset between L2WS(Fp), L2WS(Reg), GNN and DR-GD-NN.

Instance		Cold Start	L2WS(Fp)		L2WS(Reg)		GNN		DR-GD-NN	
		Iters.	Iters. ↓	Ratio ↑	Iters. ↓	Ratio ↑	Iters. ↓	Ratio ↑	Iters. ↓	Ratio ↑
QP (RHS)	200	3,855	3,616	6.2%	<b>2,018</b>	<b>47.6%</b>	2,203	42.8%	2,208	42.6%
	500	10,827	10,820	0.1%	6,117	43.5%	6,350	41.3%	<b>5,907</b>	<b>45.4%</b>
	1000	24,268	24,254	0.1%	21,566	11.1%	22,416	7.6%	<b>11,266</b>	<b>53.6%/</b>

Instance		Cold Start	L2WS(Fp)		L2WS(Reg)		GNN		DR-GD-NN	
		Time (s)	Time (s) ↓	Ratio ↑	Time (s) ↓	Ratio ↑	Time (s) ↓	Ratio ↑	Time (s) ↓	Ratio ↑
QP (RHS)	200	0.470	0.490	-4.5%	0.293	37.7%	0.311	34.6%	<b>0.289</b>	<b>38.1%</b>
	500	6.800	7.348	-8.2%	4.436	34.8%	4.019	40.0%	<b>3.735</b>	<b>44.8%</b>
	1000	85.894	88.332	-2.9%	78.684	8.1%	79.9	7.3%	<b>40.160</b>	<b>53.5%</b>

**QP.** In this section, we compare the performance of GNN and DR-GD-NN, both of which are trained in a supervised manner, using the loss function defined in Section 4.3. Since both methods are agnostic to the parameterization of the problems, we evaluate their performance on the dataset **QP** across different problem sizes. The columns labeled “Cold Start Iters.”/ “Cold Start Time (s)” and “Iters.”/ “Time (s)” denote the average number of iterations taken by the SCS solver with cold start and warm start points provided by the two methods, respectively, using the same configuration as in the previous section. The “Ratio” column represents the average ratio of reduction in the number of iterations and total time respectively. GNN and DR-GD-NN achieve similar performance on smaller datasets with 200 variables. However, DR-GD-NN performs significantly better than GNN on larger datasets with 500 and 1000 variables. This trend is consistent with the results in Table 3, where both methods show comparable performance on smaller problems but DR-GD-NN demonstrates greater scalability and efficiency in learning effective warm-start points for the SCS solver on larger-scale problems.

Table 4: Comparison of results on **QP** dataset between GNN and DR-GD-NN.

Instance	Cold Start		GNN		DR-GD-NN	
	Iters.		Iters. ↓	Ratio ↑	Iters. ↓	Ratio ↑
<b>QP</b>	200	4,568	3,200	29.9%	3,168	<b>30.6%</b>
	500	10,507	10,432	0.5%	8,768	<b>16.4%</b>
	1000	12,660	12,672	0.3%	10,862	<b>14.1%</b>

---

Instance	Cold Start		GNN		DR-GD-NN	
	Time (s)		Time (s) ↓	Ratio ↑	Time (s) ↓	Ratio ↑
<b>QP</b>	200	0.554	0.427	23.4%	0.406	<b>26.7%</b>
	500	6.591	6.701	-0.19%	5.517	<b>16.1%</b>
	1000	21.543	21.889	-1.1%	18.639	<b>13.0%</b>

**QPLIB and Portfolio.** In this section, we evaluate the performance of DR-GD-NN on larger datasets, including instances from QPLIB and synthetic portfolio optimization problems. For these experiments, we use the default settings of SCS, as outlined in Table 6, to highlight the practical warm-start effect of our approach.

To evaluate performance, we analyze the warm-start effect in terms of both solving time and the number of iterations. The columns labeled “OSQP” and “SCS” present the solve time and iteration count for the two solvers under cold-start conditions. The column “SCS (Warm Start)” includes the number of iterations required by SCS after utilizing the warm-start points, the inference time of DR-GD-NN, and the solve time, along with the total time, labeled as “Iters.”, “Inf. Time (s)”, “Solve Time (s)”, and “Time (s)” respectively. The ratio of improvement on the total time and number of iterations are included in the column “Ratio”. The observed reduction in iterations ranges from 33.7% to 57.8%, demonstrating that the warm-start points generated by DR-GD-NN enable robust performance, even on more challenging instances.

While the model inference time increases with problem size, it remains negligible compared to the solve time, especially for larger-scale problems. The reduction in solve time ranges from 8.5% to 55.7%. For the **Portfolio** dataset with 100 factors and the **QPLIB** instance 3913, the improvement in solve time is minimal compared to other cases. This is attributed to the relatively small size of these problems and their inherently short solve times. Consequently, even with a significant reduction in the number of iterations, the overall improvement in solve time is limited.

Table 5: Performance of DR-GD Net on **QPLIB** and **Portfolio** datasets.

Instance	OSQP		SCS		SCS (Warm Start)			Ratio	
	Time (s)	Iters.	Time (s)	Iters.	Inf. Time (s)	Solve Time (s)	Time (s)	Iters.	Time
<b>QPLIB</b>	3913	0.043	262	0.037	98	0.003	0.031	<b>0.034</b>	62.5% 8.9%
	4270	<b>0.744</b>	5,677	1.693	2,705	0.007	0.816	0.823	57.8% 55.7%
	8845	2.328	10,519	2.771	5,393	0.004	1.445	<b>1.449</b>	40.3% 39.0%
	3547	5.886	29,690	6.283	17,286	0.011	3.655	<b>3.666</b>	37.5% 37.3%
<b>Portfolio</b>	100	0.155	654	0.150	428	0.004	0.132	<b>0.136</b>	33.7% 8.5%
	200	0.411	997	0.626	545	0.005	0.363	<b>0.368</b>	45.0% 40.8%
	300	1.056	1,272	1.656	734	0.007	1.007	<b>1.014</b>	42.2% 38.6%
	400	2.183	1,533	4.280	712	0.010	2.140	<b>2.150</b>	53.4% 49.6%

### 5.3 Analysis of Loss and Iteration Improvement

Figure (2a) provides a detailed analysis of the relationship between validation loss and iteration improvement ratio over training epochs for the dataset **Portfolio** with 100 factors. The figure demonstrates that the validation loss steadily decreases as training progresses, indicating that the DR-GD-NN model is effectively learning to generate high-quality warm-start points. Simultaneously, the iteration improvement ratio

increases as the loss decreases, suggesting a strong correlation between the proximity of the predicted solutions to the ground-truth solutions and the models warm-starting efficiency. This trend highlights how the predicted warm-start points, as they approach the optimal solutions, lead to a decrease in the number of SCS solver iterations required, thereby enhancing the solvers overall efficiency.

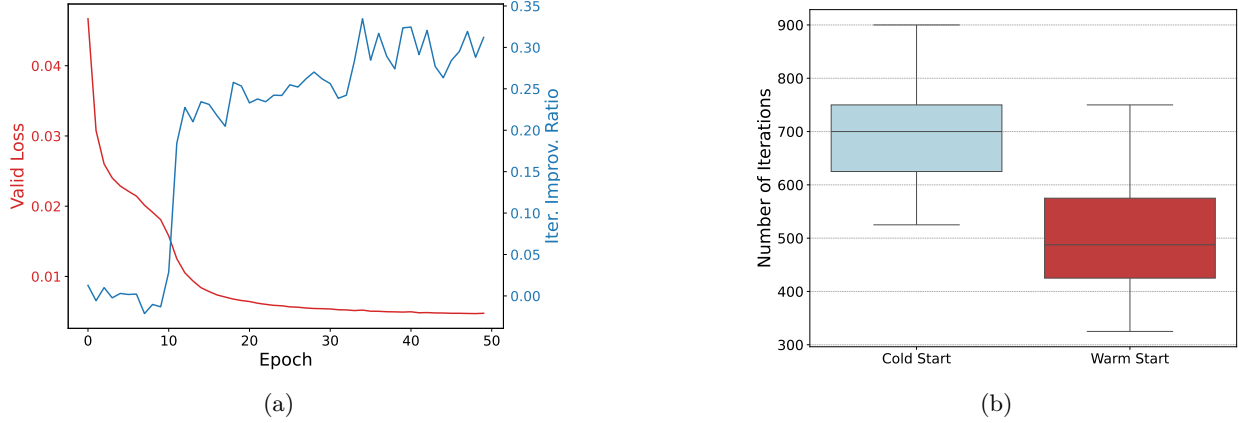


Figure 2: (a) Validation loss and iteration improvement ratio on the dataset **Portfolio** with 100 factors during training. (b) Box plot of the number of iterations required for cold starts and warm starts on the testing samples of the dataset **Portfolio** with 100 factors.

Additionally, Figure (2b) presents a box plot comparing the distribution of solver iterations required for cold starts and warm starts across all test samples. The clear separation between the distributions highlights the consistent and significant warm-start effect throughout the testing dataset. Specifically, the median number of iterations required after warm-starting is significantly lower than that for cold-starting, with a noticeably narrower interquartile range. This reduced variability suggests that DR-GD-NN not only enhances average solver performance but also contributes to more stable and predictable solver behavior.

## 6 Conclusions

In this work, we introduce the DR-GD Net, an unrolled neural network model based on a modified DR splitting algorithm, which eliminated the need for exact linear system solving at each iteration. The proposed architecture can effectively learn QP solutions and serves as a high-quality warm-start mechanism for SCS, a state-of-the-art first-order solver for convex QPs. Empirical results demonstrate that the proposed framework consistently reduces both the number of iterations and solve times across a range of problem instances. Future work will focus on integrating acceleration techniques, such as classical Anderson acceleration methods, into the unrolled network to further improve its efficiency and robustness.

## References

- Kyri Baker. Learning warm-start points for ac optimal power flow. In *2019 IEEE 29th International Workshop on Machine Learning for Signal Processing (MLSP)*, pp. 1–6. IEEE, 2019.
- Stephen Boyd and Lieven Vandenbergh. *Convex optimization*. Cambridge university press, 2004.
- Stephen Boyd, Enzo Busseti, Steve Diamond, Ronald N Kahn, Kwangmoo Koh, Peter Nystrup, Jan Speth, et al. Multi-period trading via convex optimization. *Foundations and Trends® in Optimization*, 3(1):1–76, 2017.
- Tianlong Chen, Xiaohan Chen, Wuyang Chen, Howard Heaton, Jialin Liu, Zhangyang Wang, and Wotao Yin. Learning to optimize: A primer and a benchmark. *Journal of Machine Learning Research*, 23(189): 1–59, 2022.

- Ziang Chen, Xiaohan Chen, Jialin Liu, Xinshang Wang, and Wotao Yin. Expressive power of graph neural networks for (mixed-integer) quadratic programs. *arXiv preprint arXiv:2406.05938*, 2024.
- Patrick L Combettes. Solving monotone inclusions via compositions of nonexpansive averaged operators. *Optimization*, 53(5-6):475–504, 2004.
- Corinna Cortes. Support-vector networks. *Machine Learning*, 1995.
- Damek Davis and Wotao Yin. Convergence rate analysis of several splitting schemes. *Splitting methods in communication, imaging, science, and engineering*, pp. 115–163, 2016.
- Frederik Diehl. Warm-starting ac optimal power flow with graph neural networks. In *33rd Conference on Neural Information Processing Systems (NeurIPS 2019)*, pp. 1–6, 2019.
- Priya L Donti, David Rolnick, and J Zico Kolter. Dc3: A learning method for optimization with hard constraints. In *International Conference on Learning Representations*, 2021.
- Jim Douglas and Henry H Rachford. On the numerical solution of heat conduction problems in two and three space variables. *Transactions of the American mathematical Society*, 82(2):421–439, 1956.
- Jonathan Eckstein and Dimitri P Bertsekas. On the douglasrachford splitting method and the proximal point algorithm for maximal monotone operators. *Mathematical Programming*, 55:293–318, 1992.
- Stephen Frank and Steffen Rebennack. An introduction to optimal power flow: Theory, formulation, and examples. *IIE transactions*, 48(12):1172–1197, 2016.
- Fabio Furini, Emiliano Traversi, Pietro Belotti, Antonio Frangioni, Ambros Gleixner, Nick Gould, Leo Liberti, Andrea Lodi, Ruth Misener, Hans Mittelman, et al. Qplib: a library of quadratic programming instances. *Mathematical Programming Computation*, 11:237–265, 2019.
- Xi Gao, Jinxin Xiong, Akang Wang, Qihong Duan, Jiang Xue, and Qingjiang Shi. Ipm-lstm: A learning-based interior point method for solving nonlinear programs. In *The Thirty-eighth Annual Conference on Neural Information Processing Systems*, 2024.
- Carlos E Garcia, David M Prett, and Manfred Morari. Model predictive control: Theory and practicea survey. *Automatica*, 25(3):335–348, 1989.
- Maxime Gasse, Simon Bowly, Quentin Cappart, Jonas Charfreitag, Laurent Charlin, Didier Chételat, Antonia Chmiela, Justin Dumouchelle, Ambros Gleixner, Aleksandr M Kazachkov, et al. The machine learning for combinatorial optimization competition (ml4co): Results and insights. In *NeurIPS 2021 competitions and demonstrations track*, pp. 220–231. PMLR, 2022.
- Karol Gregor and Yann LeCun. Learning fast approximations of sparse coding. In *Proceedings of the 27th international conference on international conference on machine learning*, pp. 399–406, 2010.
- Bingsheng He and Xiaoming Yuan. On the convergence rate of douglas-rachford operator splitting method. *Mathematical Programming*, 153(2):715–722, 2015.
- Jeffrey Ichnowski, Paras Jain, Bartolomeo Stellato, Goran Banjac, Michael Luo, Francesco Borrelli, Joseph E Gonzalez, Ion Stoica, and Ken Goldberg. Accelerating quadratic optimization with reinforcement learning. *Advances in Neural Information Processing Systems*, 34:21043–21055, 2021.
- Haewon Jung, Junyoung Park, and Jinkyoo Park. Learning context-aware adaptive solvers to accelerate quadratic programming. *arXiv preprint arXiv:2211.12443*, 2022.
- Diederik P Kingma. Adam: A method for stochastic optimization. *arXiv preprint arXiv:1412.6980*, 2014.
- Bingheng Li, Linxin Yang, Yupeng Chen, Senmiao Wang, Qian Chen, Haitao Mao, Yao Ma, Akang Wang, Tian Ding, Jiliang Tang, et al. Pdhg-unrolled learning-to-optimize method for large-scale linear programming. In *Forty-first International Conference on Machine Learning*, 2024.

- Haihao Lu and Jinwen Yang. A practical and optimal first-order method for large-scale convex quadratic programming. *arXiv preprint arXiv:2311.07710*, 2023.
- Harry Markowitz. Portfolio selection, 1952.
- Vishal Monga, Yuelong Li, and Yonina C Eldar. Algorithm unrolling: Interpretable, efficient deep learning for signal and image processing. *IEEE Signal Processing Magazine*, 38(2):18–44, 2021.
- Yurii Nesterov and Arkadii Nemirovskii. *Interior-point polynomial algorithms in convex programming*. SIAM, 1994.
- Jorge Nocedal and Stephen J Wright. *Numerical optimization*. Springer, 1999.
- Brendan O’Donoghue. Operator splitting for a homogeneous embedding of the linear complementarity problem. *SIAM Journal on Optimization*, 31(3):1999–2023, 2021.
- Rajiv Sambharya, Georgina Hall, Brandon Amos, and Bartolomeo Stellato. End-to-end learning to warm-start for real-time quadratic optimization. In *Learning for Dynamics and Control Conference*, pp. 220–234. PMLR, 2023.
- Rajiv Sambharya, Georgina Hall, Brandon Amos, and Bartolomeo Stellato. Learning to warm-start fixed-point optimization algorithms. *Journal of Machine Learning Research*, 25(166):1–46, 2024.
- Bartolomeo Stellato, Goran Banjac, Paul Goulart, Alberto Bemporad, and Stephen Boyd. Osqp: An operator splitting solver for quadratic programs. *Mathematical Programming Computation*, 12(4):637–672, 2020.
- Rongchao Sun, Yiqing Zhang, Hanying Zheng, Jianhua Guo, Jianyong Sun, and Jiang Xue. A douglas-rachford splitting approach based deep network for mimo signal detection. In *2023 IEEE Wireless Communications and Networking Conference (WCNC)*, pp. 1–6. IEEE, 2023.
- Robert Tibshirani. Regression shrinkage and selection via the lasso. *Journal of the Royal Statistical Society Series B: Statistical Methodology*, 58(1):267–288, 1996.
- Shobha Venkataraman and Brandon Amos. Neural fixed-point acceleration for convex optimization. In *8th ICML Workshop on Automated Machine Learning (AutoML)*.
- Philip Wolfe. The simplex method for quadratic programming. *Econometrica: Journal of the Econometric Society*, pp. 382–398, 1959.
- Xingyu Xie, Jianlong Wu, Guangcan Liu, Zhisheng Zhong, and Zhouchen Lin. Differentiable linearized admm. In *International Conference on Machine Learning*, pp. 6902–6911. PMLR, 2019.
- Linxin Yang, Bingheng Li, Tian Ding, Jianghua Wu, Akang Wang, Yuyi Wang, Jiliang Tang, Ruoyu Sun, and Xiaodong Luo. An efficient unsupervised framework for convex quadratic programs via deep unrolling. *arXiv preprint arXiv:2412.01051*, 2024.
- Ling Zhang and Baosen Zhang. Learning to solve the ac optimal power flow via a lagrangian approach. In *2022 North American Power Symposium (NAPS)*, pp. 1–6, 2022. doi: 10.1109/NAPS56150.2022.10012237.

## A Proof of Proposition 1

Our goal is to prove that the sequence generated by Algorithm 2 converges to the solution of problem (2). The proof will contain two parts:

- First, we will prove that Algorithm 2 is convergent.
- Second, we will prove that Algorithm 2 converges to the solution of problem (2).

**Lemma 2.** *Rewrite Algorithm 2 as  $w^{k+1} = T_k(w^k)$ , where  $T_k = \frac{1}{2}(Id + C_{N_C}(2\Phi_k - Id))$ . Assume  $\bigcap_{k \in \mathbb{N}} \text{Fix } T_k \neq \emptyset$ , then  $\sum_{k \in \mathbb{N}} \|T_k(w^k) - w^k\|^2 < +\infty$ , which implies that  $\|w^{k+1} - w^k\| \rightarrow 0$*

*Proof.* The Algorithm 2 can be rewritten as

$$w^{k+1} = T_k(w^k) = w^k + \left[ \frac{1}{2}(Id + C_{N_C}(2\Phi_k - Id))w^k - w^k \right], \quad (5)$$

where

$$\Phi_k(w) = (I - \eta^k(I + M)^\top(I + M)) \tilde{u}^k + \eta^k(I + M)^\top(w - q)$$

and  $C_{N_C}$  is the Cayley operator.

Since  $\|\Phi_k(w_1) - \Phi_k(w_2)\| \leq \eta^k \|I + M\| \|w_1 - w_2\|$ ,  $\Phi_k$  is Lipschitz continuous with constant  $L^k = \eta^k \lambda_{\max}(I + M)$ . Also, as

$$\langle \Phi_k(w_1) - \Phi_k(w_2), w_1 - w_2 \rangle = \langle \eta^k(I + M)^\top(w_1 - w_2), w_1 - w_2 \rangle \geq \eta^k \lambda_{\min}(I + M) \|w_1 - w_2\|^2,$$

$\Phi_k$  is strongly monotone with constant  $m^k = \eta^k \lambda_{\min}(I + M)$ .

$$\begin{aligned} & \|2\Phi_k(w_1) - w_1 - (2\Phi_k(w_2) - w_2)\|^2 \\ &= \|2(\Phi_k(w_1) - \Phi_k(w_2)) - (w_1 - w_2)\|^2 \\ &= 4\|\Phi_k(w_1) - \Phi_k(w_2)\|^2 - 4\langle \Phi_k(w_1) - \Phi_k(w_2), w_1 - w_2 \rangle + \|w_1 - w_2\|^2 \\ &\leq (4(L^k)^2 - 4m^k + 1) \|w_1 - w_2\|^2 \end{aligned}$$

If  $4(L^k)^2 - 4m^k + 1 < 1$ , that is  $m^k > (L^k)^2$ , then  $2\Phi_k - Id$  is nonexpansive and contractive.

Assume that by using line-search such that  $\eta^k < \frac{\lambda_{\min}(I+M)}{\lambda_{\max}^2(I+M)}$ , then  $2\Phi_k - Id$  is nonexpansive and thus

$$T_k = \frac{1}{2}(Id + C_A(2\Phi_k - Id)) \in \mathcal{A}\left(\frac{1}{2}\right)$$

is an averaged operator. As (5) taking the form of Algorithm 1.2 in Combettes (2004) with  $\lambda_k = 1$ ,  $e_k = 0$  and  $\alpha_k = \frac{1}{2}$ , according to Theorem 3.1 and Remark 3.4 in Combettes (2004) we can conclude that  $\sum_{k \in \mathbb{N}} \|T_k(w^k) - w^k\|^2 < +\infty$ , and thus  $\|w^{k+1} - w^k\| \rightarrow 0$   $\square$

**Corollary 3** (Corollary 5.2 Combettes (2004)). *Let  $\gamma \in (0, \infty)$ , let  $\{\nu_k\}$  be a sequence in  $(0, 2)$ , and let  $\{a_k\}$  and  $\{b_k\}$  be a sequence in  $\mathcal{H}$ . Suppose that  $0 \in A + B$  is feasible,  $\sum_{k \in \mathbb{N}} \nu_k(2 - \nu_k) = +\infty$ , and  $\sum_{k \in \mathbb{N}} \nu_k(\|a_k\| + \|b_k\|) < +\infty$ . Take  $x_0 \in \mathcal{H}$  and set  $\forall k \in \mathbb{N}$*

$$x_{k+1} = x_k + \nu_k R_{\gamma A} (2(R_{\gamma B} x_k + b_k) - x_k) + a_k - (R_{\gamma B} x_k + b_k),$$

where  $R_{\gamma A} = (Id + \gamma A)^{-1}$ ,  $R_{\gamma B} = (Id + \gamma B)^{-1}$  are the resolvents for  $A$  and  $B$ . Then  $\{x_k\}$  converges weakly to some point  $x \in \mathcal{H}$  and  $R_{\gamma B} x \in (A + B)^{-1}(0)$ .

**Proposition 1** The sequence  $\{u^k\}$  generated by Algorithm 2 converges to the solution of problem (2). Furthermore, the sequences  $\{x^k\}$  and  $\{y^k\}$  also converge to the solution of problem (1).

*Proof.* From (5), let  $\Phi_k = R_F + \epsilon^k$ , where  $\epsilon^k$  represents the error induced by the inexact evaluation of the resolvent of  $F$ . Therefore, the Algorithm 2 can be rewritten as

$$\begin{aligned} w^{k+1} &= T_k(w^k) = \frac{1}{2}(Id + C_{N_C}(2\Phi_k - Id))w^k \\ &= \frac{1}{2}w^k + R_{N_C}(2\Phi_k - Id)w^k - \frac{1}{2}(2\Phi_k - Id)w^k \\ &= w^k + R_{N_C}(2R_F(w^k) - w^k) - (R_F(w^k) + \epsilon^k) \end{aligned}$$

By taking  $x_k = w^k, a_k = 0, b_k = \epsilon^k, \gamma = 1, \nu_k = 1$  and let  $A = R_{N_C}$  and  $B = F$ , Algorithm 2 is taking the form of (3). To prove the Proposition 1, we are left to show that  $\sum_{k \in \mathbb{N}} \|\epsilon^k\| < +\infty$ .

Let  $f_k(\tilde{u}) = \frac{1}{2}\|(I + M)\tilde{u} - (w^k - q)\|^2$ , line 4–5 in Algorithm 2 can be written as

$$\tilde{u}^{k+1} = \tilde{u}^k - \eta^k \nabla f_k(\tilde{u}^k)$$

where the step size  $\eta^k$  is chosen to satisfy the *Wolfe conditions* (Nocedal & Wright, 1999), that is

$$f_k(\tilde{u}^k) - f_k(\tilde{u}^{k+1}) \geq c_1 \eta^k \|\nabla f_k(\tilde{u}^k)\|^2 \quad (6)$$

$$\nabla f_k(\tilde{u}^{k+1})^\top \nabla f_k(\tilde{u}^k) \leq c_2 \|\nabla f_k(\tilde{u}^k)\|^2, \quad (7)$$

where  $c_1$  and  $c_2$  are the parameters for the line search and  $0 < c_1 < c_2 < 1$ .

From (7), we have

$$(\nabla f_k(\tilde{u}^{k+1}) - \nabla f_k(\tilde{u}^k))^\top \nabla f_k(\tilde{u}^k) \leq (c_2 - 1) \|\nabla f_k(\tilde{u}^k)\|^2.$$

$f_k$  is Lipschitz continuous with constant  $L = \sigma_{\max}(I + M)$ , as  $\|\nabla f_k(x) - \nabla f_k(y)\| \leq L\|x - y\|$ . Therefore

$$\begin{aligned} & -(\nabla f_k(\tilde{u}^{k+1}) - \nabla f_k(\tilde{u}^k))^\top \nabla f_k(\tilde{u}^k) \\ & \leq |(\nabla f_k(\tilde{u}^{k+1}) - \nabla f_k(\tilde{u}^k))^\top \nabla f_k(\tilde{u}^k)| \\ & \leq \|(\nabla f_k(\tilde{u}^{k+1}) - \nabla f_k(\tilde{u}^k))\| \|\nabla f_k(\tilde{u}^k)\| \\ & \leq \eta^k L \|\nabla f_k(\tilde{u}^k)\|^2, \end{aligned}$$

which implies that

$$\begin{aligned} \eta^k &\geq -\frac{(\nabla f_k(\tilde{u}^{k+1}) - \nabla f_k(\tilde{u}^k))^\top \nabla f_k(\tilde{u}^k)}{L \|\nabla f_k(\tilde{u}^k)\|^2} \\ &\geq \frac{(1 - c_2) \|\nabla f_k(\tilde{u}^k)\|^2}{L \|\nabla f_k(\tilde{u}^k)\|^2} = \frac{1 - c_2}{L}. \end{aligned}$$

Therefore

$$f_k(\tilde{u}^k) - f_k(\tilde{u}^{k+1}) \geq c_1 \eta^k \|\nabla f_k(\tilde{u}^k)\|^2 \geq c_1 \frac{1 - c_2}{L} \|\nabla f_k(\tilde{u}^k)\|^2.$$

Since  $f_k(\tilde{u}) \geq 0$

$$1 - \frac{f_k(\tilde{u}^{k+1})}{f_k(\tilde{u}^k)} \geq c_1 \frac{1 - c_2}{L} \frac{\|\nabla f_k(\tilde{u}^k)\|^2}{f_k(\tilde{u}^k)} \geq 2c_1 \frac{1 - c_2}{L} \sigma_{\min}(I + M),$$

where  $\sigma_{\min}(I + M) \geq 1$  is the minimum singular value of  $(I + M)$ . (As  $M + M' \succeq 0$ , the real parts of the eigenvalues of  $M$  are nonnegative.)

The last inequality is from:

$$\nabla f_k(\tilde{u}^k) = (I + M)^\top ((I + M)\tilde{u}^k - (w^k - q))$$

$$\begin{aligned}
& \frac{\|\nabla f_k(\tilde{u}^k)\|^2}{f_k(\tilde{u}^k)} \\
&= 2 \frac{\left((I+M)\tilde{u}^k - (w^k - q)\right)^\top (I+M)(I+M)^\top \left((I+M)\tilde{u}^k - (w^k - q)\right)}{\|(I+M)\tilde{u}^k - (w^k - q)\|^2} \\
&\geq 2\lambda_{\min} \left((I+M)(I+M)^\top\right), \quad (\text{rayleigh quotient}) \\
&= 2\sigma_{\min}(I+M).
\end{aligned}$$

From Lemma 2,  $\sum_{k \in \mathbb{N}} \|w^{k+1} - w^k\|^2 < +\infty$  and  $\|w^{k+1} - w^k\| \rightarrow 0$ . Let us further assume that  $\eta^k$  also satisfies the assumption in Lemma 2, then  $\exists K$ , such that  $\forall k > K$   $\Phi_{k+1} \approx \Phi_k$  and  $2\Phi_k - Id$  is contractive. Therefore,  $\forall k > K, \exists 0 < c < 1$ , such that  $\|w^{k+1} - w^k\| \leq c\|w^k - w^{k-1}\|$  and thus  $\sum_{k=K}^\infty \|w^{k+1} - w^k\| < +\infty$ . As  $\sum_{k \in \mathbb{N}} \|w^{k+1} - w^k\|^2 < +\infty$ ,  $\sum_{k=0}^{K-1} \|w^{k+1} - w^k\|$  is bounded. We can conclude that  $\sum_{k \in \mathbb{N}} \|w^{k+1} - w^k\| < +\infty$ .

Defining  $\tau^k = \frac{f_k(\tilde{u}^{k+1})}{f_k(\tilde{u}^k)}$  and taking  $0 < c_1 < \frac{1}{2} < c_2 < 1$ , then

$$\tau^k = \frac{f_k(\tilde{u}^{k+1})}{f_k(\tilde{u}^k)} \leq 1 - 2c_1 \frac{1 - c_2}{L} \sigma_{\min}(I+M) = 1 - 2c_1(1 - c_2) \frac{\sigma_{\min}(I+M)}{\sigma_{\max}(I+M)} := \tau < 1.$$

Therefore

$$\|(I+M)\tilde{u}^{k+1} - (w^k - q)\| \leq \tau \|(I+M)\tilde{u}^k - (w^k - q)\|.$$

$$\begin{aligned}
\|\epsilon^k\| &= \|\tilde{u}^{k+1} - (I+M)^{-1}(w^k - q)\| \\
&\leq \|(I+M)^{-1}\| \|(I+M)\tilde{u}^{k+1} - (w^k - q)\| \\
&\leq \|(I+M)^{-1}\| \tau \|(I+M)\tilde{u}^k - (w^k - q)\| \\
&\leq \|(I+M)^{-1}\| \tau \|(I+M)\tilde{u}^k - (w^{k-1} - q) + (w^{k-1} - q) - (w^k - q)\| \\
&\leq \|(I+M)^{-1}\| (\tau^2 \|(I+M)\tilde{u}^{k-1} - (w^{k-1} - q)\| + \tau \|w^k - w^{k-1}\|) \\
&\leq \dots \\
&\leq \|(I+M)^{-1}\| (\tau^{k+1} \|(I+M)\tilde{u}^0 - (w^0 - q)\| + \sum_{j=1}^k \tau^{k-j+1} \|w^j - w^{j-1}\|) \\
&:= \|(I+M)^{-1}\| \left( \sum_{j=0}^k \tau^{k-j+1} \|w^j - w^{j-1}\| \right), \quad (\text{denote } w^{(-1)} = (I+M)\tilde{u}^0) \\
&:= \|(I+M)^{-1}\| a_k.
\end{aligned}$$

Next, we prove the convergence of  $\sum_{k \in \mathbb{N}} \|\epsilon^k\|$  by showing the convergence of  $\sum_{k \in \mathbb{N}} a_k$ .

$$\begin{aligned}
\sum_{k \in \mathbb{N}} a_k &= \sum_{k=0}^{\infty} a_k = \sum_{k=0}^{\infty} \sum_{j=0}^k \tau^{k-j+1} \|w^j - w^{j-1}\| \\
&= \sum_{j=0}^{\infty} \|w^j - w^{j-1}\| \sum_{k=j}^{\infty} \tau^{k+1-j} \\
&= \sum_{j=0}^{\infty} \|w^j - w^{j-1}\| \tau \sum_{k=0}^{\infty} \tau^k \\
&= \sum_{j=0}^{\infty} \|w^j - w^{j-1}\| \frac{\tau}{1 - \tau} < +\infty,
\end{aligned}$$

Therefore,  $\sum_{k \in \mathbb{N}} \|\epsilon^k\| \leq \sum_{k=0}^{\infty} a_k < +\infty$ . Then according to Corollary 3, we can conclude that  $\exists w^*$ , such that  $w^k \rightharpoonup w^*$ . As in a finite-dimensional space strong convergence and weak convergence are equivalent, we can conclude that  $w^k \rightarrow w^*$ . In addition,  $u^* = \tilde{u}^* = R_F(w^*) \in (F + N_C)^{-1}(0)$ .  $\square$



## B SCS Settings

The parameter settings for SCS in the experiments are listed in Table 6:

Table 6: Solver configurations.

Instance	data scaling	dual scale factor	adapt dual scale	primal scale factor	alpha	acceleration lookback	acceleration interval
QP (RHS)/QP	False	1	False	1	1	0	0
QPLIB/Portfolio	True	0.1	True	$10^{-6}$	1.5	10	10